

PROPERTIES OF ANISOTROPIC PHOTONIC BAND GAPS IN THREE-DIMENSIONAL PLASMA PHOTONIC CRYSTALS CONTAINING THE UNIAXIAL MATERIAL WITH DIFFERENT LATTICES

Hai-Feng Zhang^{1, 2, *}, Shao-Bin Liu^{1, †}, and Xiang-Kun Kong¹

¹College of Electronic and Information Engineering, Nanjing University of Aeronautics and Astronautics, Nanjing 210016, P. R. China

²Nanjing Artillery Academy, Nanjing 211132, P. R. China

Abstract—In this paper, the properties of anisotropic photonic band gaps (PBGs) in three-dimensional (3D) nonmagnetized plasma photonic crystals (PPCs) composed of anisotropic dielectric (the uniaxial material) spheres immersed in uniform nonmagnetized plasma background with various lattices including the diamond, face-centered-cubic (fcc), body-centered-cubic (bcc) and simple-cubic (sc) lattices, are theoretically investigated by the plane wave expansion (PWE) method. The equations for calculating the anisotropic PBGs in the first irreducible Brillouin zone are theoretically deduced. The anisotropic PBGs and a flatbands region can be obtained as the uniaxial material introduced into 3D PPCs. The PPCs with diamond lattices consisting of isotropic dielectric have the larger PBGs compared to PPCs doped by the uniaxial material since its low-symmetry structure. Furthermore, the PPCs with fcc, bcc, sc lattices will not exhibit a complete PBG unless the uniaxial material is introduced. The influences of the ordinary-refractive index, extraordinary-refractive index, filling factor and plasma frequency external magnetic field on the properties of anisotropic PBGs for 3D PPCs with fcc, bcc, sc lattices are investigated in detail, respectively, and some corresponding physical explanations are also given. The numerical results show that the anisotropy can open partial band gaps in 3D PPCs with fcc, bcc, sc lattices, and the complete PBGs can be obtained compared to 3D PPCs doped by the conventional isotropic dielectric. It also is shown that

Received 17 May 2013, Accepted 22 June 2013, Scheduled 18 July 2013

* Corresponding author: Hai-Feng Zhang (hanlor@163.com).

† The second author Shao-bin Liu has made a similar contribution to the first author.

the anisotropic PBGs can be tuned by the ordinary-refractive index, extraordinary-refractive index, filling factor and plasma frequency, respectively. The complete PBGs can be obtained by introducing the uniaxial material as 3D PPCs are with high-symmetry lattices. This also provides a way to design the tunable devices.

1. INTRODUCTION

The photonic crystals (PCs) have been extensively investigated in theory and experiment since the pioneering work of Yablonovitch [1] and John [2] in 1987. The most attractive feature of PCs is their photonic band gaps (PBGs) [3], where electromagnetic (EM) waves cannot propagate for any polarizations along any direction. The larger PBGs can be used to design the many important applications [4–7]. During past a few years, intensive studies have been mainly concerned with the conventional dielectric materials. In recently, PCs comprising the dispersive materials such as plasma [8], superconductor [9] and metallic [10] have become increasing important. PCs with plasma components have been attracted the great attentions of researchers since the idea of plasma photonic crystals (PPCs) firstly proposed by Hojo and Mase [11]. The plasma can be looked as metamaterial [12], and also can be controlled by some external agents [13]. Compared to the conventional dielectric PCs, the PPCs have some interesting properties on the dispersion such as larger PBGs [14], the tunable PBGs [15] and tunable photonic defect states [16]. They also can be used to design the tunable devices [17–19]. Up to now, the one- and two-dimensional (2D) PPCs have achieved rapid development in theoretical and experimental research [20–22]. For 1D PPCs, Guo [23] theoretically investigated the dispersion and transmission properties of 1D PPCs, and found the PBGs can be tuned by the plasma parameters. The properties of transmission and defect modes of 1D magnetized PPCs are studied by Liu et al. [24] and Zhang et al. [25] based on finite-difference time-domain (FDTD) method, respectively. Zhang et al. [26, 27] used 1D PPCs to design the omnidirectional reflector by a matching layer and fractal heterostructure techniques. They found 1D PPCs is good candidate to enhance the omnidirectional band gaps. The transmission characteristics of 1D magnetized PPCs with dielectric defect layer were investigated by Qi et al. [28] based on the transfer matrix method (TMM). They found that defect modes can be modulated by the magnetized plasma in a larger frequency region. Zhang et al. [29] considered a more general case. They studied the dispersive properties of 1D magnetized PPCs with arbitrary magnetic declination, and found that the PBGs can be notably tuned by the

parameters of magnetized PPCs. The magnetized coupled resonator PPCs and plasma-magnetic PCs are investigated by Hamidi [30] and Mehdian et al. [31]. For 2D case, Qi [32] investigated the dispersion for 2D magnetized PPCs by plane wave expansion (PWE) method, and found that the PBGs can be tuned by the parameters of magnetized plasma. Zhang et al. [33, 34] studied the transmission and defect mode properties of 2D PPCs for TM wave by FDTD method, and pointed out that the PBGs and defect mode can be tuned by plasma frequency, host dielectric constant and filling factor, respectively. Fu et al. [35] analyzed the dispersion relation of magnetic plasma-metal PCs based on FDTD method, and found that the positions of the flat bands, cutoff frequency, and PBGs can be controlled by the external magnetic field, respectively. On the other hand, Zhang et al. [36] and Qi and Zhang [37] arranged plasma periodically by the external magnetic field to form a new kind of 2D and 1D magnetized PPCs, which are only composed of the plasma, and proclaimed that the PBGs also can be tuned by the external magnetic field.

As mentioned above, the most of published reports about PPCs focus on 1D and 2D cases until Zhang et al. [38–40] proposed the properties of PBGs for 3D nonmagnetized PPCs with diamond and simple-cubic (sc) lattices. The same research group also investigated the dispersive properties of 3D magnetized PPCs [41, 42]. As mentioned in their works [38, 41], 3D PPCs with sc lattices will suffer from high-symmetry lattices and dielectric constant of dielectric must be sufficiently large so that the resonant scattering of EM waves is prominent enough to open a band gap [43]. Unfortunately, technological difficulties can be found in fabricating the 3D PPCs to obtain the complete PBGs with large dielectric constant of dielectric. Therefore, if we want to achieve the complete PBGs in 3D magnetized plasma photonic crystals (MPPCs) with high symmetry lattices, we have to break the high symmetry [44] and use anisotropic dielectric to realize the PCs [45]. To our knowledge, it is difficult to achieve the complete PBGs as the PCs with high-symmetry lattices such as face-centered-cubic (fcc), body-centered-cubic (bcc) and sc lattices [43]. The previous reports on the 3D PPCs always considered the filling dielectric is isotropic. The anisotropic PBGs of 3D PPCs with high-symmetry lattices are rarely investigated. Therefore, the aim of the present paper is to perform a systematic study of the anisotropic PBGs in 3D PPCs with high-symmetry lattices (fcc, bcc and sc) doped by the anisotropic dielectric (uniaxial material) based on a modified PWE method. The proposed 3D PPCs are that the anisotropic dielectric spheres are immersed in the nonmagnetized plasma background periodically with various lattices. This paper is organized

as follows. The equations of computing the anisotropic PBGs for the 3D PPCs with various lattices are theoretically deduced in Section 2. In Section 3, the influences of the ordinary-refractive index, extraordinary-refractive index, filling factor and plasma frequency on the properties of anisotropic PBGs for 3D PPCs with fcc, bcc and sc lattices are studied, respectively. Finally, conclusions are given in Section 4. An $e^{j\omega t}$ time-dependence is implicit through the paper, with t the time, and $j = \sqrt{-1}$. We also consider c is light speed in vacuum.

2. THEORETICAL MODEL AND NUMERICAL METHOD

The standard Brillouin zone and schematic structures of 3D PPCs with a spherical atom in simple lattice such as diamond, bcc, fcc and sc lattices can be found in many textbooks and reports [38–43]. Thus, they are not shown here. We assumed the radius of the sphere and lattice constant are R and a , respectively. The relative dielectric function for nonmagnetized plasma is ε_p and it is homogeneous. As we know, the nonmagnetized plasma is a kind of frequency dependence dielectric, the dielectric function ε_p that meets the Drude model and can be written as [13]:

$$\varepsilon_p(\omega) = 1 - \frac{\omega_p^2}{\omega(\omega - j\nu_c)} \quad (1)$$

where ω_p , ν_c , and ω are the plasma frequency, plasma collision frequency, and EM wave frequency, respectively. Plasma frequency $\omega_p = (e^2 n_e / \varepsilon_0 m)^{1/2}$ in which e , m , n_e and ε_0 are electron charge, electric mass, plasma density and dielectric constant in vacuum, respectively.

In order to obtain the anisotropic photonic band structure of 3D PPCs, several efficient numerical methods have been reported, such as the PWE [32], the FDTD [26, 27], the TMM [28], the plane-wave-based transfer-matrix [46], the cell [47], the moving least squares [48], the multidomain pseudospectral [49] and the spectral element methods [50]. The PWE method is the most popular method to achieve the band structure. Especially, Zhang et al. [51] proposed a modified PWE technique, which can calculate successfully the PBGs for the PCs composed of the Drude-type medium. As mentioned in Ref. [51], a standard linearization technique was used to solve the general nonlinear eigenvalue equation. Thus, the PCs composed of the frequency dependence dielectric could be calculated easily by such method. In this paper, the same technique also will be used to obtain

the anisotropic PBGs of 3D PPCs with different (fcc, bcc and sc) lattices containing the uniaxial material.

As we know, the uniaxial material [43] has two different principal-refractive indices known as ordinary-refractive and extraordinary-refractive indices, which can found in the nature. We consider the ordinary-refractive and extraordinary-refractive indices are n_o and n_e , respectively. For the anisotropic material, the dielectric constant $\epsilon_{\mathbf{a}}$ is a dyadic and can be written as

$$\epsilon_{\mathbf{a}} = \begin{pmatrix} \epsilon_x & 0 & 0 \\ 0 & \epsilon_y & 0 \\ 0 & 0 & \epsilon_z \end{pmatrix} \quad (2)$$

where

$$\epsilon_x = n_x^2, \quad \epsilon_y = n_y^2, \quad \epsilon_z = n_z^2.$$

Therefore, for the uniaxial material, the dielectric dyadic has only three cases for diagonal element permutation as [43] (a) $n_x = n_e, n_y = n_z = n_o$; (b) $n_y = n_e, n_x = n_z = n_o$; (c) $n_z = n_e, n_x = n_y = n_o$. We name them type-1, type-2 and type-3 uniaxial materials, respectively. In order to simplify, we just deduce the equations for calculating the anisotropic PBGs of 3D PPCs containing the type-1 uniaxial material. For the type-1 case, the $\epsilon_{\mathbf{a}}^{-1}$ is the inverse dyadic of $\epsilon_{\mathbf{a}}$ and can be written as

$$\epsilon_{\mathbf{a}}^{-1} = \begin{pmatrix} \epsilon_x^{-1} & 0 & 0 \\ 0 & \epsilon_y^{-1} & 0 \\ 0 & 0 & \epsilon_y^{-1} \end{pmatrix} \quad (3)$$

On the other hand, the Maxwell's equation for the magnetic field in 3D PPCs can be expressed as:

$$\nabla \times \left[\frac{1}{\epsilon(\mathbf{r})} \nabla \times \mathbf{H} \right] = -\frac{\omega^2}{c^2} \mathbf{H} \quad (4)$$

Since $\epsilon(\mathbf{r})$ is periodic, we can use Bloch's theorem to expand the \mathbf{H} field in term of plane wave,

$$\mathbf{H}(\mathbf{r}) = \sum_{\mathbf{G}} \sum_{\lambda=1}^2 h_{\mathbf{G},\lambda} \hat{\mathbf{e}}_{\lambda} e^{j(\mathbf{k}+\mathbf{G})\cdot\mathbf{r}} \quad (5)$$

where \mathbf{k} is a wave vector in the Brillouin zone of lattice, \mathbf{G} is a reciprocal-lattice vector, and $\hat{\mathbf{e}}_1, \hat{\mathbf{e}}_2$ are orthogonal unit vectors that are both perpendicular to wave vector $\mathbf{k} + \mathbf{G}$ because of the transverse character of magnetic field \mathbf{H} (i.e., $\nabla \cdot \mathbf{H} = 0$). The dielectric constant dyadic can also be expanded into its Fourier form as

$$\epsilon^{-1}(\mathbf{r}) = \sum_{\mathbf{G}} \epsilon_{\mathbf{a}}^1(\mathbf{G}) e^{j\mathbf{G}\cdot\mathbf{r}} \quad (6)$$

where the Fourier transform coefficient $\varepsilon_{\mathbf{a}}^{-1}$ is also a dyadic. Substituting Eq. (5) and Eq. (6) into Eq. (4), the following linear matrix equations can be obtained

$$\sum_{\mathbf{G}', \lambda'} H_{\mathbf{G}, \mathbf{G}'}^{\lambda, \lambda'} h_{\mathbf{G}', \lambda'} = \frac{\omega^2}{c^2} h_{\mathbf{G}, \lambda} \quad (7)$$

where

$$H_{\mathbf{G}, \mathbf{G}'}^{\lambda, \lambda'} = |\mathbf{k} + \mathbf{G}| |\mathbf{k} + \mathbf{G}'| \begin{pmatrix} \hat{\mathbf{e}}_2 \cdot \varepsilon_{\mathbf{G}, \mathbf{G}'}^{-1} \cdot \hat{\mathbf{e}}_{2'} & -\hat{\mathbf{e}}_2 \cdot \varepsilon_{\mathbf{G}, \mathbf{G}'}^{-1} \cdot \hat{\mathbf{e}}_{1'} \\ -\hat{\mathbf{e}}_1 \cdot \varepsilon_{\mathbf{G}, \mathbf{G}'}^{-1} \cdot \hat{\mathbf{e}}_{2'} & \hat{\mathbf{e}}_1 \cdot \varepsilon_{\mathbf{G}, \mathbf{G}'}^{-1} \cdot \hat{\mathbf{e}}_{1'} \end{pmatrix} \quad (8)$$

In order to solve the Eq. (7), we can rewrite the Eq. (3) as

$$\begin{aligned} \varepsilon_{\mathbf{a}}^{-1} &= \begin{pmatrix} \varepsilon_x^{-1} & 0 & 0 \\ 0 & \varepsilon_y^{-1} & 0 \\ 0 & 0 & \varepsilon_y^{-1} \end{pmatrix} = \varepsilon_x^{-1} \begin{pmatrix} 1 & 0 & 0 \\ 0 & 0 & 0 \\ 0 & 0 & 0 \end{pmatrix} + \varepsilon_y^{-1} \begin{pmatrix} 0 & 0 & 0 \\ 0 & 1 & 0 \\ 0 & 0 & 1 \end{pmatrix} \\ &= \varepsilon_x^{-1} \overleftrightarrow{\mathbf{I}}_x + \varepsilon_y^{-1} \overleftrightarrow{\mathbf{I}}_y \end{aligned} \quad (9)$$

where

$$\overleftrightarrow{\mathbf{I}}_x = \begin{pmatrix} 1 & 0 & 0 \\ 0 & 0 & 0 \\ 0 & 0 & 0 \end{pmatrix}, \quad \overleftrightarrow{\mathbf{I}}_y = \begin{pmatrix} 0 & 0 & 0 \\ 0 & 1 & 0 \\ 0 & 0 & 1 \end{pmatrix}.$$

Thus, the Eq. (8) can be rewritten as

$$\begin{aligned} &H_{\mathbf{G}, \mathbf{G}'}^{\lambda, \lambda'} \\ &= |\mathbf{k} + \mathbf{G}| |\mathbf{k} + \mathbf{G}'| \sum_{i=x, y} \begin{pmatrix} \hat{\mathbf{e}}_2 \cdot \overleftrightarrow{\mathbf{I}}_i \cdot \hat{\mathbf{e}}_{2'} & -\hat{\mathbf{e}}_2 \cdot \overleftrightarrow{\mathbf{I}}_i \cdot \hat{\mathbf{e}}_{1'} \\ -\hat{\mathbf{e}}_1 \cdot \overleftrightarrow{\mathbf{I}}_i \cdot \hat{\mathbf{e}}_{2'} & \hat{\mathbf{e}}_1 \cdot \overleftrightarrow{\mathbf{I}}_i \cdot \hat{\mathbf{e}}_{1'} \end{pmatrix} \cdot \varepsilon_{\mathbf{G}, \mathbf{G}'}^{-1}(i) \end{aligned} \quad (10)$$

where $\varepsilon_{\mathbf{G}, \mathbf{G}'}^{-1}(i)$ are the Fourier transform coefficients for ε_x^{-1} and ε_y^{-1} , respectively. As we know, the dielectric sphere filling factor can be written as $f = (4\pi R^3)/(3V_m)$, V_m is the volume of unit cell. The Fourier coefficients $\varepsilon_{\mathbf{G}, \mathbf{G}'}^{-1}(i)$ could be written as [38–40]:

$$\varepsilon_{\mathbf{G}, \mathbf{G}'}^{-1}(i) = \begin{cases} \left(\frac{\omega^2 - j\nu_c \omega}{\omega^2 - j\nu_c \omega - \omega_p^2} \right) (1 - f) + \left(\frac{1}{\varepsilon_i} \right) f, & \mathbf{G} = 0 \\ \left(\frac{1}{\varepsilon_i} - \left(\frac{\omega^2 - j\nu_c \omega}{\omega^2 - j\nu_c \omega - \omega_p^2} \right) \right) 3f \left(\frac{\sin(|\mathbf{G}|R) - (|\mathbf{G}|R) \cos(|\mathbf{G}|R)}{(|\mathbf{G}|R)^3} \right), & \mathbf{G} \neq 0 \end{cases} \quad (i = x, y) \quad (11)$$

We can write $h_{\mathbf{G}, \lambda}$ of $\mathbf{H}(\mathbf{r})$ in the form [38–40]

$$h_{\mathbf{G}, \lambda} = \sum_{\mathbf{G}} A(\mathbf{k}|\mathbf{G}) e^{j(\mathbf{K} + \mathbf{G}) \cdot \mathbf{r}} \quad (12)$$

We can obtain as the equation for the coefficients $\{A(\mathbf{k}|\mathbf{G})\}$

$$\begin{aligned}
 & (\varepsilon_a^{-1}) \cdot |\mathbf{k} + \mathbf{G}| |\mathbf{k} + \mathbf{G}'| \cdot \vec{\mathbf{F}} \cdot A(\mathbf{k}|\mathbf{G}) + \sum_{\mathbf{G}'} \varepsilon_a^{-1} \cdot |\mathbf{k} + \mathbf{G}| |\mathbf{k} + \mathbf{G}'| \cdot \vec{\mathbf{F}} \cdot A(\mathbf{k}|\mathbf{G}) \\
 & = \frac{\omega^2}{c^2} A(\mathbf{k}|\mathbf{G})
 \end{aligned} \tag{13}$$

where the prime on the sum over \mathbf{G}' indicates that the term with $\mathbf{G}' = \mathbf{G}$ is omitted. We consider $\vec{\mathbf{F}}_x = \begin{pmatrix} \hat{\mathbf{e}}_2 \cdot \overleftrightarrow{\mathbf{I}}_x \cdot \hat{\mathbf{e}}_{2'} & -\hat{\mathbf{e}}_2 \cdot \overleftrightarrow{\mathbf{I}}_x \cdot \hat{\mathbf{e}}_{1'} \\ -\hat{\mathbf{e}}_1 \cdot \overleftrightarrow{\mathbf{I}}_x \cdot \hat{\mathbf{e}}_{2'} & \hat{\mathbf{e}}_1 \cdot \overleftrightarrow{\mathbf{I}}_x \cdot \hat{\mathbf{e}}_{1'} \end{pmatrix}$,

$$\vec{\mathbf{F}}_y = \begin{pmatrix} \hat{\mathbf{e}}_2 \cdot \overleftrightarrow{\mathbf{I}}_y \cdot \hat{\mathbf{e}}_{2'} & -\hat{\mathbf{e}}_2 \cdot \overleftrightarrow{\mathbf{I}}_y \cdot \hat{\mathbf{e}}_{1'} \\ -\hat{\mathbf{e}}_1 \cdot \overleftrightarrow{\mathbf{I}}_y \cdot \hat{\mathbf{e}}_{2'} & \hat{\mathbf{e}}_1 \cdot \overleftrightarrow{\mathbf{I}}_y \cdot \hat{\mathbf{e}}_{1'} \end{pmatrix} \text{ and } \vec{\mathbf{F}} = \vec{\mathbf{F}}_x + \vec{\mathbf{F}}_y, \text{ respectively.}$$

At this point we use the definition of a complex variable μ given by

$$\mu = \omega/c \tag{14}$$

Eq. (13) yields

$$\mu^4 \vec{\mathbf{I}} - \mu^3 \vec{\mathbf{T}} - \mu^2 \vec{\mathbf{U}} - \mu \vec{\mathbf{V}} - \vec{\mathbf{W}} = 0 \tag{15}$$

where $\vec{\mathbf{I}}$ is the identity matrix, and

$$\vec{\mathbf{T}}(\mathbf{G}|\mathbf{G}') = j \frac{\nu_c}{c} \delta_{\mathbf{G}, \mathbf{G}'}, \tag{16a}$$

$$\begin{aligned}
 \vec{\mathbf{U}}(\mathbf{G}|\mathbf{G}') & = \left\{ \sum_{i=x,y} \left(\frac{\omega_p^2}{c^2} + \left(\frac{1}{\varepsilon_i} f + (1-f) \right) \cdot |\mathbf{k} + \mathbf{G}|^2 \cdot \overleftrightarrow{\mathbf{F}}_i \right) \right\} \delta_{\mathbf{G}, \mathbf{G}'} \\
 & + \sum_{i=x,y} \left(\frac{1}{\varepsilon_i} - 1 \right) \overleftrightarrow{\mathbf{M}}_i,
 \end{aligned} \tag{16b}$$

$$\begin{aligned}
 \vec{\mathbf{V}}(\mathbf{G}|\mathbf{G}') & = \left\{ \sum_{i=x,y} \left(-j \frac{\nu_c}{c} \left(\frac{1}{\varepsilon_i} f + (1-f) \right) \cdot |\mathbf{k} + \mathbf{G}|^2 \cdot \overleftrightarrow{\mathbf{F}}_i \right) \right\} \delta_{\mathbf{G}, \mathbf{G}'} \\
 & + \sum_{i=x,y} -j \frac{\nu_c}{c} \left(\frac{1}{\varepsilon_i} - 1 \right) \overleftrightarrow{\mathbf{M}}_i,
 \end{aligned} \tag{16c}$$

$$\begin{aligned}
 \vec{\mathbf{W}}(\mathbf{G}|\mathbf{G}') & = \left\{ \sum_{i=x,y} \left(-\frac{\omega_p^2}{c^2} \frac{f}{\varepsilon_i} \cdot |\mathbf{k} + \mathbf{G}|^2 \cdot \overleftrightarrow{\mathbf{F}}_i \right) \right\} \delta_{\mathbf{G}, \mathbf{G}'} \\
 & + \sum_{i=x,y} \frac{\omega_p^2}{c^2} \left(1 - \frac{1}{\varepsilon_i} \right) \overleftrightarrow{\mathbf{M}}_i,
 \end{aligned} \tag{16d}$$

where $\overleftrightarrow{\mathbf{M}}_i = |\mathbf{k} + \mathbf{G}|^2 \cdot \overleftrightarrow{\mathbf{F}} \cdot 3f\left(\frac{\sin(|\mathbf{G}|R) - (|\mathbf{G}|R)\cos(|\mathbf{G}|R)}{(|\mathbf{G}|R)^3}\right)$ ($i = x, y$), the element of the $N \times N$ matrices are $\overleftrightarrow{\mathbf{T}}$, $\overleftrightarrow{\mathbf{U}}$, $\overleftrightarrow{\mathbf{V}}$ and $\overleftrightarrow{\mathbf{W}}$. This polynomial form can be transformed into a linear problem in $4N$ dimension by $\overleftrightarrow{\mathbf{Q}}$ that fulfills

$$\overleftrightarrow{\mathbf{Q}}z = \mu z, \quad \overleftrightarrow{\mathbf{Q}} = \begin{bmatrix} \mathbf{0} & \overleftrightarrow{\mathbf{I}} & \mathbf{0} & \mathbf{0} \\ \mathbf{0} & \mathbf{0} & \overleftrightarrow{\mathbf{I}} & \mathbf{0} \\ \mathbf{0} & \mathbf{0} & \mathbf{0} & \overleftrightarrow{\mathbf{I}} \\ \overleftrightarrow{\mathbf{W}} & \overleftrightarrow{\mathbf{V}} & \overleftrightarrow{\mathbf{U}} & \overleftrightarrow{\mathbf{T}} \end{bmatrix} \quad (17)$$

The complete solution of Eq. (6) is obtained by solving for the eigenvalues of Eq. (17). Of course the dispersion relation can be determined by the real part of such eigenvalues. The analogue equation to Eq. (10) for another two types of cases also can be easily derived.

3. NUMERICAL RESULTS AND DISCUSSION

In our calculation, we adopt a total number of 729 plane waves, and the convergence accuracy is better than 1% for the lower energy bands for diamond, fcc, bcc and sc lattices [43], respectively. Without loss of generality, we plot $\omega a/2\pi c$ with the normalization convention $\omega_{p0}a/2\pi c = 1$. The symbol ω_{p0} is a variable, and its value is $2\pi c/a$. Thus, we can define the plasma frequency as $\omega_p = 0.3\pi c/a = 0.15\omega_{p0}$ to make the problem scale-invariant. With this definition, we can let a take any value as long as R is shifted according to achieve the same filling factor. In our calculation, we also choose the plasma collision frequency as $\nu_c = 0.02\omega_{pl}$ and $f = 0.25$, respectively. The plasma is a kind of dispersive medium and can be looked as metamaterial. The properties of plasma can be easily tuned by the external magnetic field, plasma density and the temperature of plasma, respectively. Therefore, the PPCs can be used to design the novel tunable devices, such as tunable filter [16], omnidirectional reflector [18] and polarization splitter [19]. As we know, the electron plasma density n_e is located in 10^{12} – 10^{16} cm^{-3} [12], which corresponds to electron plasma frequency $\omega_p/2\pi = 10$ – 1000 GHz, that means plasma PC can dynamically control electromagnetic waves from microwaves to THz waves. If a is equal to 0.003 m, the $\omega_{p0}/2\pi$ is equal to 10 GHz. If a is equal to 0.0003 m, the $\omega_{p0}/2\pi$ is equal to 1000 GHz. Thus, the value of $\omega_p/2\pi$ runs from 1.5 to 150 GHz according to the definition of plasma frequency as mentioned in our manuscript. The plasma collision frequency ν_c is located in 30 MHz–3 GHz. In this paper, we consider the plasma frequency is equal to 30 GHz and the plasma collision frequency ν_c is 0.6 GHz. The

value of a is chosen as 0.0015 m. We only focus on the first (1st) PBGs for 3D PPCs in various lattices. In order to investigate the anisotropic PBGs of 3D PPCs, the relative bandwidth is defined as

$$\Delta\omega/\omega_i = 2(\omega_{up} - \omega_{low})/(\omega_{up} + \omega_{low}) \quad (18)$$

where ω_{up} and ω_{low} are the upper and lower limits of a PBG, respectively.

3.1. The Anisotropic PBGs of 3D PPCs Containing the Uniaxial Material in Various Lattices

To investigate the effects of anisotropy, space topology on the complete PBGs, we plot the band structures of 3D PPCs with diamond lattices containing the uniaxial material and isotropic dielectric in Fig. 1, respectively. As we know, the high-symmetry points in the Brillouin zone have the coordinate as $\Gamma = (0, 0, 0)$, $X = (2\pi/a, 0, 0)$, $W = (2\pi/a, \pi/a, 0)$, $K = (1.5\pi/a, 1.5\pi/a, 0)$, $L = (\pi/a, \pi/a, \pi/a)$, and $U = (2\pi/a, 0.5\pi/a, 0.5\pi/a)$. As shown in Figs. 1(a)–(c), the complete PBGs can be obtained as 3D PPCs doped by three types of uniaxial materials, and the 1st PBGs present themselves at 0.5134–0.5235 ($2\pi c/a$), 0.4198–0.4334 ($2\pi c/a$) and 0.5115–0.5179 ($2\pi c/a$), respectively. The value of $2\pi c/a$ is equal to 200 GHz. The relative bandwidths are 0.0195, 0.0319 and 0.0124, respectively. The 3D PPCs with diamond lattices consisting of type-2 uniaxial material have largest relative bandwidth compared to another two types of uniaxial material. As a comparison, we also present the band diagram of 3D PPCs containing isotropic dielectric in Fig. 1(d). As shown in the Fig. 1(d), the 1st PBG runs from 0.4586 to 0.4787 ($2\pi c/a$), and the relative bandwidth is 0.0429. One can compare Figs. 1(a)–(c) with the photonic band structure of such isotropic PBG, and all of relative bandwidths obtained by the uniaxial material are less than that for such isotropic PBG. This can be explained in physics that the diamond lattice is not a high-symmetry structure in topology, and the anisotropy does not help to enlarge or achieve the complete PBGs. As mentioned above, enlarging the PBGs by the reduction of crystal symmetry by anisotropic anisotropy is not a good choice, since the asymmetry of diamond lattice provides a better way to open the band gaps at high-symmetry points in the Brillouin zone. However, for the other simpler lattices such as fcc, bcc and sc lattices, the complete PBGs can be obtained by the introduction of anisotropic dielectric into the 3D PPCs. In Fig. 2, we plot anisotropic photonic band structure of 3D PPCs containing the isotropic material in various lattices as $n_z = n_x = n_y = 4.8$, $\omega_p = 0.15\omega_{p0}$, $\nu_c = 0.02\omega_{p1}$, and $f = 0.25$. As we know, the high-symmetry points in the Brillouin zone for fcc lattices are same as in the diamond structure. For the bcc

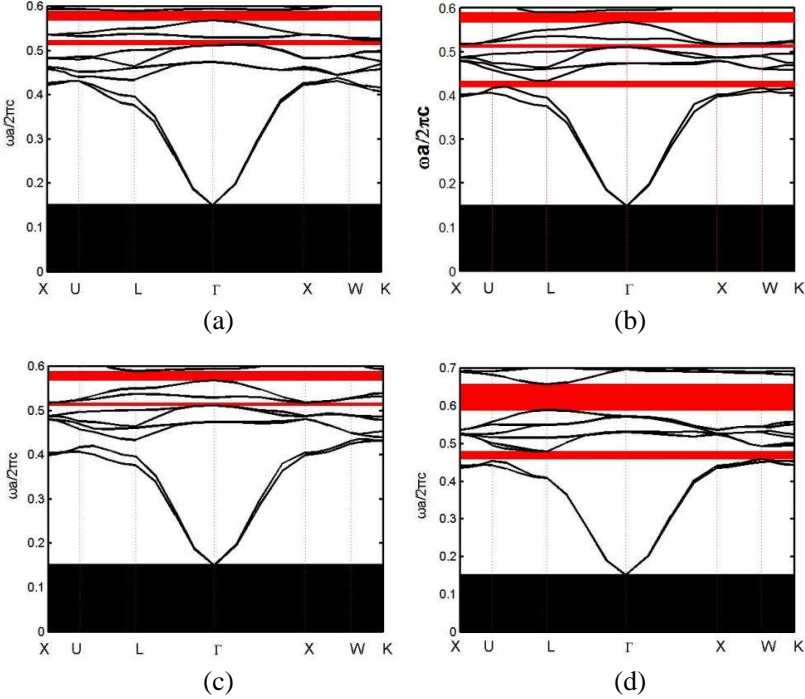


Figure 1. Calculated anisotropic photonic band structure of 3D PPCs with diamond lattices as $f = 0.25$, $\omega_p = 0.15\omega_{p0}$, $\nu_c = 0.02\omega_{p1}$, and (a) $n_x = n_e = 6.2$, $n_y = n_z = n_o = 4.8$; (b) $n_y = n_e = 6.2$, $n_x = n_z = n_o = 4.8$; (c) $n_z = n_e = 6.2$, $n_x = n_y = n_o = 4.8$; and (d) $n_z = n_e = 4.8$, $n_x = n_y = n_o = 4.8$, respectively. (d) The photonic structure for 3D PCs consists of isotropic dielectric spheres in air background as $n_z = n_x = n_y = 4.8$ and $f = 0.25$.

lattices, the high-symmetry points are $\Gamma = (0, 0, 0)$, $H = (0, 0, 2\pi/a)$, $N = (0, \pi/a, \pi/a)$ and $P = (\pi/a, \pi/a, \pi/a)$. For the sc lattices, the high-symmetry points are $\Gamma(0, 0, 0)$, $X = (\pi/a, 0, 0)$, $M = (\pi/a, \pi/a, 0)$, and $R = (\pi/a, \pi/a, \pi/a)$.

It is clearly seen that the complete PBGs can not be found in Fig. 2 since band degeneracy at some high-symmetry points, which are W and U points for a fcc lattice, H and P points for a bcc lattice, and M and R points for a sc lattice. This can be explained by the high symmetry of those lattices and the dielectric constant of dielectric is not large enough to open a band gap [43]. If we want to achieve the complete PBGs, the uniaxial material such as Te (tellurium) can

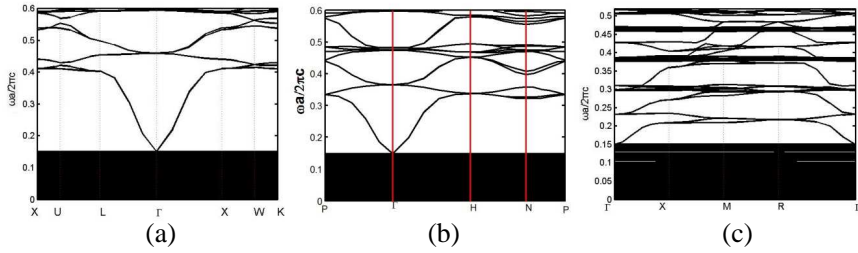


Figure 2. Calculated anisotropic photonic band structure of 3D PPCs containing the isotropic material with various lattices as $n_z = n_x = n_y = 4.8$, $\omega_p = 0.15\omega_{p0}$, $\nu_c = 0.02\omega_{p1}$, and $f = 0.25$. (a) fcc lattices, (b) bcc lattices, and (c) sc lattices, respectively.

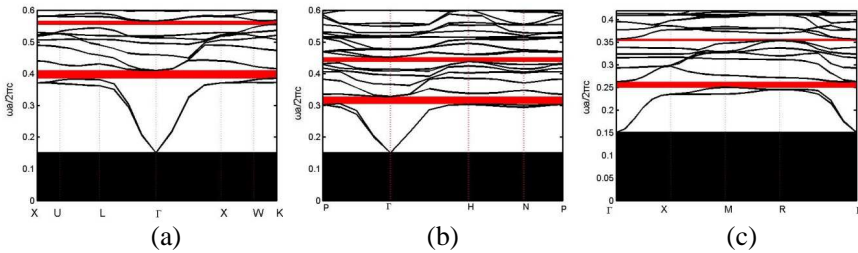


Figure 3. Calculated anisotropic photonic band structure of 3D PPCs containing the type-1 uniaxial material with various lattices as $n_x = n_e = 6.2$, $n_y = n_z = n_o = 4.8$, $\omega_p = 0.15\omega_{p0}$, $\nu_c = 0.02\omega_{p1}$, and $f = 0.25$. (a) fcc lattices, (b) bcc lattices, and (c) sc lattices, respectively.

be used to form 3D PPCs. Te is a kind of positive uniaxial crystals with principal-refractive indices $n_e = 6.2$ and $n_o = 4.8$. In Fig. 3, we plot the band structure of 3D PPCs containing the type-1 uniaxial material in various lattices as $f = 0.25$, $\omega_p = 0.15\omega_{p0}$ and $\nu_c = 0.02\omega_{p1}$, respectively. Fig. 3 reveals that the complete PBGs can be obtained and flatbands regions appear by introducing the uniaxial material as 3D PPCs in various lattices. There exist the flatbands regions because of the existence of surface plasmon modes, which stem from the coupling effects between the plasma. In the flatbands, the group velocity is very slow. The 1st PBGs for fcc, bcc and sc lattices are located at $0.3855\text{--}0.4106 (2\pi c/a)$, $0.3053\text{--}0.3281 (2\pi c/a)$ and $0.2502\text{--}0.2626 (2\pi c/a)$, and the relative bandwidths are 0.0631, 0.072 and 0.0484, respectively. Compared to fcc and sc lattices, the 1st PBG for

bcc lattices has largest bandwidth. Similarly, the band structure of 3D PPCs containing type-2 and type-3 uniaxial materials in similar case to Fig. 2 are plotted in Figs. 4 and 5, respectively. One can see from Fig. 4 that the 1st PBGs are covered $0.3969\text{--}0.3992$ ($2\pi c/a$), $0.3079\text{--}0.3166$ ($2\pi c/a$) and $0.2586\text{--}0.2626$ ($2\pi c/a$) ($2\pi c/a$), and the relative bandwidths are 0.0058, 0.0279 and 0.0154, respectively. It also can see from Fig. 5 that there do not exist the PBGs as 3D PPCs with bcc and sc lattices but the PBG of fcc structure runs from 0.3969 to 0.3992 ($2\pi c/a$). Comparing the results in Figs. 3–5 lead us to infer that the uniaxial material induced splitting of the lowest bands above the flatbands regions are so remarkable and make them can open band gaps at high-symmetry points. Compared to another two uniaxial

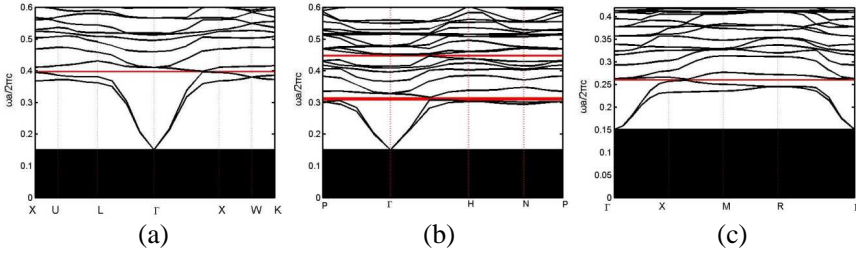


Figure 4. Calculated anisotropic photonic band structure of 3D PPCs containing the type-2 uniaxial material with various lattices as $n_y = n_e = 6.2$, $n_x = n_z = n_o = 4.8$, $\omega_p = 0.15\omega_{p0}$, $\nu_c = 0.02\omega_{p1}$, and $f = 0.25$. (a) fcc lattices, (b) bcc lattices, and (c) sc lattices, respectively.

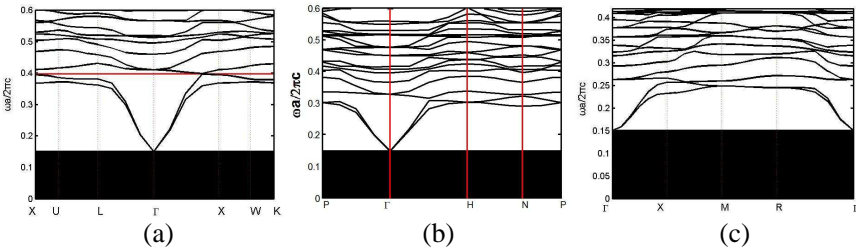


Figure 5. Calculated anisotropic photonic band structure of 3D PPCs containing the type-3 uniaxial material with various lattices as $n_z = n_e = 6.2$, $n_x = n_y = n_o = 4.8$, $\omega_p = 0.15\omega_{p0}$, $\nu_c = 0.02\omega_{p1}$, and $f = 0.25$. (a) fcc lattices, (b) bcc lattices, and (c) sc lattices, respectively.

materials, 3D PPCs consisting of type-1 uniaxial materials in fcc, bcc and sc lattices have largest bandwidths and relative bandwidths of 1st PBGs. As mentioned above, introduced the anisotropic dielectric into 3D PPCs can enlarge and obtain the complete PBGs only in the case of PPCs with high-symmetry lattices. The largest bandwidths and relative bandwidths of PBGs can be achieved as type-1 uniaxial material is introduced.

3.2. Influences of the Extraordinary-refractive Index on Anisotropic PBGs

In Fig. 6(a), we plot the 1st anisotropic PBGs of 3D PPCs with fcc, bcc and sc lattices as a function of the extraordinary-refractive index with $f = 0.25$, $\omega_p = 0.15\omega_{p0}$, $\nu_c = 0.02\omega_{p1}$ and $n_o = 4.8$, respectively. The shaded regions indicate the PBGs. As show in Fig. 6(a), the edges of 1st PBGs shift downward to lower frequencies, and the frequency range increase first then decrease with increasing n_e . The 1st PBGs for fcc, bcc and sc lattices will never appear as n_e is less than 5.3, 5.5 and 5, respectively. As n_e is increased from 5 to 9, the 1st PBGs located at $0.3434\text{--}0.3605 (2\pi c/a)$, $0.2858\text{--}0.2983 (2\pi c/a)$, and $0.2235\text{--}0.2321 (2\pi c/a)$, respectively. The bandwidths of 1st PBGs for fcc and bcc lattices are increased by 0.0108 and $0.0086 (2\pi c/a)$ compared to the cases of $n_e = 5.3$ and 5.5 , respectively. However, the frequency range for sc lattices is decreased by $0.0002 (2\pi c/a)$ compared to the case of $n_e = 5$. There exists an optimal n_e , which make the maximum

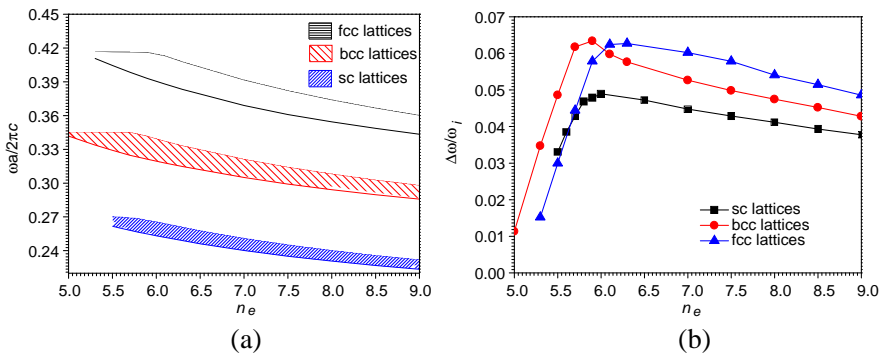


Figure 6. The influences of extraordinary-refractive index n_e on the 1st PBGs and relative bandwidths for 3D PPCs with various lattices as $f = 0.25$, $\omega_p = 0.15\omega_{p0}$, $\nu_c = 0.02\omega_{p1}$, and $n_o = 4.8$, respectively. The shaded regions indicate the PBGs. (a) The 1st PBGs, and (b) relative bandwidths.

bandwidths of 1st PBG for various lattices also can be obtained. The relative bandwidths ($\Delta\omega/\Delta\omega_i$) of 1st PBGs for fcc, bcc and sc lattices also are plotted in Fig. 6(b). Fig. 6(b) illustrates that the general trends for the 1st PBGs for various lattices are relative bandwidths increase first then decrease with increasing n_e . The maximum relative bandwidths of 1st PBGs for fcc, bcc and sc lattices are 0.0627, 0.0634 and 0.0489, which can be found at cases of $n_e = 6.3, 5.9$ and 6.1 , respectively. Compared to the case of $n_e = 9$, the relative bandwidths of such three lattices are increased by 0.0141, 0.0206 and 0.0112, respectively. Comparing the results in Fig. 6 lead us to infer that the maximum relative bandwidth of PPCs with bcc lattices is largest compared to another two lattices. The 1st PBG of fcc structure has the highest central frequency but the lowest central frequency of 1st PBG will be found in the sc lattices. This can be explained by the anisotropic properties of 3D PPCs. Changing the n_e means a sufficient anisotropy of atom dielectricity has been provided [43], and the band gap can be achieved. The PPCs with higher symmetry of lattices means the larger PBG can be obtained. As we know, the bandwidths of the PBGs are governed by refractive contrast for PCs and the positions of the PBGs are governed by the average refractive index of PCs. Thus, the average refractive index of 3D PPCs is changed as the n_e is changed. In other words, the locations of 1st PBGs can be tuned by n_e .

3.3. Influences of the Ordinary-refractive Index on Anisotropic PBGs

In Fig. 6(a), we present the 1st anisotropic PBGs of 3D PPCs with fcc, bcc and sc lattices as a function of the ordinary-refractive index with $f = 0.25$, $\omega_p = 0.15\omega_{p0}$, $\nu_c = 0.02\omega_{p1}$ and $n_e = 6.2$, respectively. The shaded regions indicate the PBGs. One can see from Fig. 7(a) that the edges of 1st PBGs for fcc, bcc and sc lattices are downward to lower frequencies, and the bandwidths increase first then decrease with increasing n_o . The 1st PBGs for bcc and sc lattices will never appear as n_o is less than 2.8 but 1st PBG for fcc lattices will appear until n_o is larger than 3.2. As n_o is increased from 2.8 to 5.5, the 1st PBGs present themselves at 0.3679–0.3589 ($2\pi c/a$), 0.297–0.2837 ($2\pi c/a$), and 0.2402–0.2335 ($2\pi c/a$), respectively. The central frequency of 1st PBG for fcc lattices is largest compared to another two lattices, and the lowest central frequency of 1st PBG can be found in sc lattices. Compared to the cases of $n_o = 2.8$ and 3.2 , the bandwidths for bcc and sc lattices are increased by 0.0005 and 0.0038 ($2\pi c/a$) but the frequency range for fcc lattices is decreased by 0.0032 ($2\pi c/a$), respectively. In Fig. 7(b), the relative bandwidths of 1st PBGs for various lattices also are plotted. As shown in Fig. 7(b), the general trends for the 1st PBGs

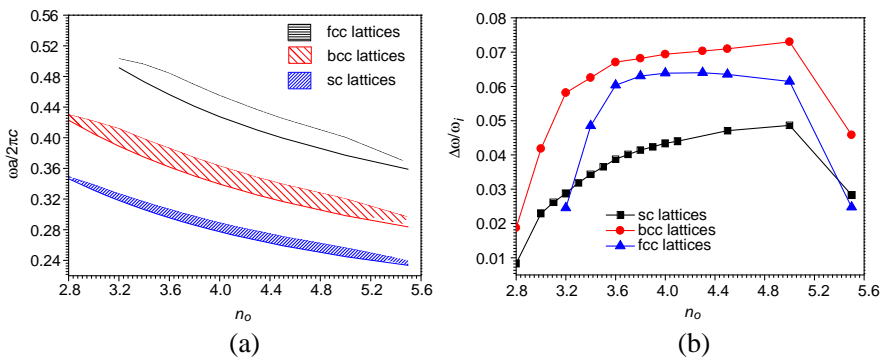


Figure 7. The influences of ordinary-refractive index n_o on the 1st PBGs and relative bandwidths for 3D PPCs with various lattices as $f = 0.25$, $\omega_p = 0.15\omega_{p0}$, $\nu_c = 0.02\omega_{p1}$, and $n_e = 6.2$, respectively. The shaded regions indicate the PBGs. (a) The 1st PBGs, and (b) relative bandwidths.

for fcc, bcc and sc lattices are relative bandwidths increase first then decrease with increasing n_o . The maximum relative bandwidths are 0.064, 0.073 and 0.0434, which can be found at cases of $n_o = 4.3$, 5 and 4, respectively. Compared to the case of $n_o = 5.5$, the relative bandwidths are increased by 0.0387, 0.0272, and 0.0203, respectively. One can see that, generally, the largest relative bandwidth can be found in the bcc lattices. Similar to changing the extraordinary-refractive index, the way to change the ordinary-refractive index of uniaxial material means that the refractive contrast and average refractive index of 3D PPCs are changed. Therefore, the 1st PBGs for various lattices can be tuned by n_o .

3.4. Influences of the Filling Factor on Anisotropic PBGs

In Fig. 8(a), we plot the dependences of the properties of 1st anisotropic PBG for fcc, bcc and sc lattices on the filling factor f with $\omega_p = 0.15\omega_{p0}$, $\nu_c = 0.02\omega_{p1}$, $n_o = 4.8$ and $n_e = 6.2$, respectively. The shaded regions indicate the PBGs. Fig. 8(a) reveals that the edges of 1st PBGs for fcc, bcc and sc lattices are downward to lower frequencies, and the frequency ranges increase first then decrease with increasing f . The 1st PBGs for fcc and bcc lattices will never appear until the f is larger 0.05. However, if f is less then 0.15 or larger than 0.4, the PBG for sc structure will disappear. As f is increased from 0.05 to 0.52, the maximum bandwidths of 1st PBGs for fcc, bcc and sc lattices are 0.0272, 0.0261, 0.0132 ($2\pi c/a$), which can be found at the

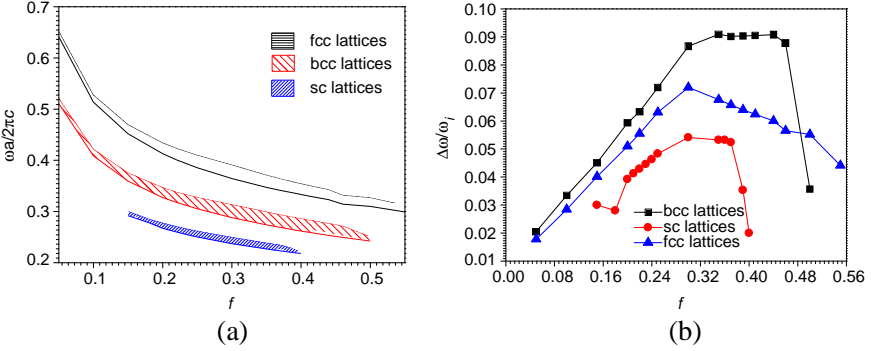


Figure 8. The influences of filling factor f on the 1st PBGs and relative bandwidths for 3D PPCs with various lattices as $\omega_p = 0.15\omega_{p0}$, $\nu_c = 0.02\omega_{p1}$, $n_o = 4.8$ and $n_e = 6.2$, respectively. The shaded regions indicate the PBGs. (a) The 1st PBGs, and (b) relative bandwidths.

cases of $f = 0.3$, 0.35 and 0.3 , respectively. Thus, the 1st PBGs for fcc, bcc and sc lattices can be tuned by f . This can be explained in physics that increasing filling factor means the space averaged dielectric constant of PPCs becoming larger [38–40]. In Fig. 8(b), we plot the relative bandwidths as a function of the filling factor. Fig. 8(b) reveals that the relative bandwidths of 1st PBGs for fcc, bcc and sc lattices increase first then decrease with increasing f . The maximum relative bandwidths for such three lattices are 0.072 , 0.091 , 0.0541 , which can be found at the cases of $f = 0.3$, 0.35 and 0.3 , respectively. Compared to the cases of $f = 0.15$, the relative bandwidths are increased by 0.0319 , 0.0458 and 0.0241 , respectively. One also can see that the largest relative bandwidth can be found in the bcc lattices. It also is noticed that if the filling factor of uniaxial material is small enough and close to null, the 3D PPCs can be looked as a plasma block. The flatbands region will disappear. As mentioned above, the PBGs of 3D PPCs with fcc, bcc and sc lattices can be tuned by the filling factor, and it also is an important parameter which need be chosen.

3.5. Influences of the Plasma Frequency on Anisotropic PBGs

In Fig. 9(a), we plot the influences of plasma frequency on the 1st anisotropic PBG for fcc, bcc and sc lattices with $f = 0.25$, $\nu_c = 0.02\omega_{p1}$, $n_o = 4.8$ and $n_e = 6.2$, respectively. The shaded regions indicate the PBGs. As shown in Fig. 9(a), the edges of 1st PBGs for fcc, bcc and sc lattices shift upward to higher frequencies, and the

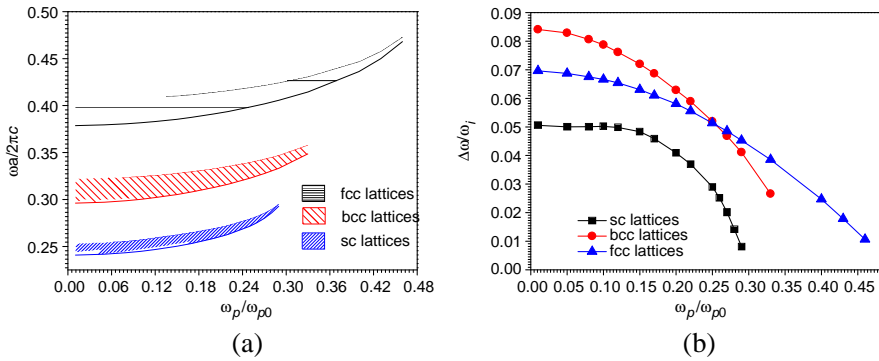


Figure 9. The influences of plasma frequency ω_p on the 1st PBGs and relative bandwidths for 3D PPCs with various lattices as $f = 0.25$, $\nu_c = 0.02\omega_{p1}$, $n_o = 4.8$ and $n_e = 6.2$, respectively. The shaded regions indicate the PBGs. (a) The 1st PBGs, and (b) relative bandwidths.

bandwidths of 1st PBGs decrease with increasing the value of ω_p/ω_{p0} . The 1st PBGs for fcc, bcc and sc lattices will disappear as the value of ω_p/ω_{p0} is larger 0.46, 0.33 and 0.29, respectively. As the value of ω_p/ω_{p0} is increased from 0.01 to 0.46, the 1st PBGs for fcc, bcc and sc lattices will disappear at $\omega_p/\omega_{p0} = 0.46, 0.33$ and 0.29 , respectively. If the value of ω_p/ω_{p0} is 0.46, the 1st PBG for fcc lattices is covered $0.4683\text{--}0.4733$ ($2\pi c/a$) and the frequency range is decreased by 0.059 ($2\pi c/a$) compared to the case of $\omega_p/\omega_{p0} = 0.01$. If the value of ω_p/ω_{p0} is 0.33, the 1st PBG for bcc lattices is located $0.3488\text{--}0.3582$ ($2\pi c/a$) and the bandwidth is decreased by 0.0575 ($2\pi c/a$) compared to the case of $\omega_p/\omega_{p0} = 0.01$. If the value of ω_p/ω_{p0} is 0.33, the 1st PBG for sc lattices is located $0.293\text{--}0.2954$ ($2\pi c/a$) and the frequency range is decreased by 0.0417 ($2\pi c/a$) compared to the case of $\omega_p/\omega_{p0} = 0.01$. The maximum frequency ranges of 1st PBGs are 0.0273, 0.026 and 0.0123, respectively, which can be found at the cases of $\omega_p/\omega_{p0} = 0.01$. It also is shown that the central frequency of 1st PBG for fcc lattices is largest compared to another two lattices, and the lowest central frequency of 1st PBG can be found in sc lattices. In Fig. 9(b), we also plot the relative bandwidths as a function of plasma frequency. Fig. 9(b) illustrates that the relative bandwidths of 1st PBGs decrease as the value of ω_p/ω_{p0} is increased from 0.01 to 0.46. The maximum relative bandwidth of 1st PBG is 0.0696, 0.0841 and 0.0506, which can be found at the cases of $\omega_p/\omega_{p0} = 0.01$, respectively. It is clearly seen that the largest relative bandwidth can be found in the bcc lattices. As mentioned above, the PBGs for fcc, bcc and sc lattices

can be manipulated by the plasma frequency. The main reason for this result is because changing plasma frequency means that the relative dielectric constant of nonmagnetized plasma also is changed. Thus, the refractive contrast and average refractive index of 3D PPCs have been changed. Consequently, the PBGs of 3D PPCs can be tuned by plasma frequency. It should be pointed out that the plasma collision frequency does not affect the PBGs and flatbands [38–40] because the dispersion relation does not present any rapid change as ν_c is small compared to ω_p . The plasma collision frequency only affects the magnitude of transmission [29].

4. CONCLUSION

In summary, the properties of anisotropic PBGs 3D PPCs composed of anisotropic dielectric (the uniaxial material) spheres immersed in uniform nonmagnetized plasma background with various lattices including the diamond, fcc, bcc and sc lattices, are theoretically investigated by the PWE method. The equations for calculating the anisotropic PBGs in the first irreducible Brillouin zone are theoretically deduced. Such method can be used to calculate 3D MPPCs with any lattices containing any anisotropic dielectric. Based on the numerical results, some conclusion can be drawn. Since low-symmetry structure in topology, the PPCs with diamond lattices consisting of isotropic dielectric have the larger PBGs compared to PPCs doped by the uniaxial material. However, the PPCs with fcc, bcc, sc lattices will not exhibit a complete PBG unless the uniaxial material is introduced. Compare with the same structure composed by the isotropic dielectric spheres in nonmagnetized plasma, the complete PBGs and a flatbands region can be obtained as the uniaxial material is introduced. The flatbands caused by the existence of surface plasmon modes which stem from the coupling effects between the magnetized plasma. The 3D PPCs with fcc, bcc and sc lattices consisting of the type-1 uniaxial material ($n_x = n_e$, $n_y = n_z = n_o$) have a larger PBG compared to 3D MPPCs doped by another two types of uniaxial materials. The central frequency of 1st PBG for fcc lattices is largest compared to another two lattices, and the lowest central frequency of 1st PBG can be found in sc lattices. The PPCs with bcc lattices have largest relative bandwidth of 1st PBG. The 1st PBGs of 3D PPCs with fcc, bcc and sc lattices can be manipulated by the extraordinary-refractive and ordinary-refractive indices, and the general trends for 1st PBGs are relative bandwidths increase first then decrease with increasing extraordinary-refractive and ordinary-refractive indices. The 1st PBGs also can be tuned notably by the plasma frequency. Increasing the plasma frequency,

the bandwidths of PBGs will decrease, and the maximum relative bandwidths can be obtained at low- ω_p region. With increasing the filling factor, the relative width and bandwidth of 1st PBG will increase first then decrease. It also is noticed that if filling factor is small enough and close to null, the 3D PPCs can be seen as a plasma block. The flatbands regions will disappear. As mentioned above, we can take advantage of the uniaxial material to obtain the complete PBGs as 3D PPCs with high-symmetry lattices. These results may provide theoretical instructions to design the tunable devices by 3D PPCs.

ACKNOWLEDGMENT

This work was supported in part by the National Natural Science Foundation of China (Grant No. 60971122), in part by Jiangsu Province Science Foundation (Grant No. BK2011727), in part by the Open Research Program in China's State Key Laboratory of Millimeter Waves (No. K201103), in part by the Fundamental Research Funds for the Central Universities and the Funding of Jiangsu Innovation Program for Graduate Education (Grant No. CXZZ11-0211).

REFERENCES

1. Yablonovitch, E., "Inhibited spontaneous emission of photons in solid-state physics and electronics," *Phys. Rev. Lett.*, Vol. 58, 2059–2061, 1987.
2. John, S., "Strong localization of photons in certain disordered dielectric superlattices," *Phys. Rev. Lett.*, Vol. 58, 2486–2489, 1987.
3. Banerjee, A., "Enhanced refractometric optical sensing by using one-dimensional ternary photonic crystals," *Progress In Electromagnetics Research*, Vol. 89, 11–22, 2009.
4. Jim, K. L., D. Y. Wang, C. W. Leung, C. L. Choy, and H. L. W. Chan, "One-dimensional tunable ferroelectric photonic crystals based on $\text{Ba}_{0.7}\text{Sr}_{0.3}\text{TiO}_3/\text{MgO}$ multilayer thin films," *J. Appl. Phys.*, Vol. 103, 083107, 2008.
5. Tanabe, T., M. Notomi, S. Mitsugi, A. Shinya, and E. Kuramochi, "Low mode volume slotted photonic crystal single nanobeam cavity," *Appl. Phys. Lett.*, Vol. 97, 151112, 2005.
6. Sirigiri, J. R., K. E. Kreischer, J. Machuzak, I. Mastovsky, M. A. Shapiro, and R. J. Temkin, "Photonic-band-gap resonator gyrotron," *Phys. Rev. Lett.*, Vol. 86, 5628, 2001.

7. Smirnova, E. I., A. S. Kesar, I. Mastovsky, M. A. Shapiro, and R. J. Temkin, "Demonstration of a 17 GHz, high-gradient accelerator with a photonic-band-gap structure," *Phys. Rev. Lett.*, Vol. 95, 074801, 2005.
8. Zhang, H. F., M. Li, and S. B. Liu, "Study periodic band gap structure of the magnetized plasma photonic crystals," *Optoelectron Lett.*, Vol. 5, 112–116, 2009.
9. Zhang, H. F., S. B. Liu, X. K. Kong, B. R. Bian, and Y. Dai, "Omnidirectional photonic band gaps enlarged by Fibonacci quasi-periodic one-dimensional ternary superconductor photonic crystals," *Solid State Commun.*, Vol. 152, 2113–2119, 2012.
10. Kuzmiak, V. and A. A. Maradudin, "Distribution of electromagnetic field and group velocities in two-dimensional periodic systems with dissipative metallic components," *Phy. Rev. B*, Vol. 58, 7230–7251, 1998.
11. Hojo, H. and A. Mase, "Dispersion relation of electromagnetic waves in one dimensional plasma photonic crystals," *Plasma Fusion Res.*, Vol. 80, 89–90, 2004.
12. Sakai, O. and K. Tachibana, "Plasma as metamaterial: A review," *Plasma Sources Sci. Technol.*, Vol. 21, 013001, 2012.
13. Ginzberg, V. L., *The Propagation of Electromagnetic Waves in Plasmas*, Pergamon, New York, 1970.
14. Qi, L. and Z. Yang, "Modified plane wave method analysis of dielectric plasma photonic crystal," *Progress In Electromagnetics Research*, Vol. 91, 319–332, 2009.
15. Guo, B., "Photonic band gap structures of obliquely incident electromagnetic wave propagation in a one-dimension absorptive plasma photonic crystal," *Phys. Plasmas*, Vol. 16, 043508, 2009.
16. Li, C., S. Liu, X. Kong, H. Zhang, B. Bian, and X. Zhang, "A novel comb-like plasma photonic crystals filter in the presence of evanescent wave," *IEEE Trans. Plasma Sci.*, Vol. 39, 1969–1973, 2011.
17. Zhang, H. F., S. B. Liu, and X. K. Kong, "Enlarged the omnidirectional band gap in one-dimensional plasma photonic crystals with ternary Thue-Morse aperiodic structure," *Physica B*, Vol. 410, 244–250, 2013.
18. Zhang, H. F., S. B. Liu, X. K. Kong, L. Zhou, C. Z. Li, and B. R. Bian, "Enlarged omnidirectional photonic photonic band gap in heterostructure of plasma and dielectric photonic crystals," *Optik*, Vol. 124, 751–756, 2013.
19. Shiverhwari, L., "Zero permittivity band characteristics in one-

- dimensional plasma dielectric photonic crystals,” *Optik*, Vol. 122, 1523–1526, 2011.
20. Sakaguchi, T., O. Sakai, and K. Tachibana, “Photonic bands in two-dimensional microplasma array II. Band gaps observed in millimeter and sub-terahertz ranges,” *J. Appl. Phys.*, Vol. 101, 073305, 2007.
 21. Sakai, O., T. Sakaguchi, and K. Tachibana, “Photonic bands in two-dimensional microplasma array I. Theoretical derivation of band structure of electromagnetic waves,” *J. Appl. Phys.*, Vol. 101, 073304, 2007.
 22. Fan, W. and L. Dong, “Tunable one-dimensional plasma photonic crystals in dielectric barrier discharge,” *Phys. Plasmas*, Vol. 17, 073506, 2010.
 23. Guo, B., “Photonic band gap structures of obliquely incident electromagnetic wave propagation in a one-dimension absorptive plasma photonic crystal,” *Phys. Plasmas*, Vol. 16, 043508, 2009.
 24. Liu, S. B., C. Q. Gu, J. J. Zhou, and N. C. Yuan, “FDTD simulation for magnetized plasma photonic crystals,” *Acta Physica Sinica*, Vol. 55, 1283–1288, 2006.
 25. Zhang, H. F., L. Ma, and S. B. Liu, “Defect mode properties of magnetized plasma photonic crystals,” *Acta Physica Sinica*, Vol. 58, 01071–01075, 2009.
 26. Zhang, H. F., S. B. Liu, X. K. Kong, L. Zou, C. Z. Li, and W. S. Qing, “Enhancement of omnidirectional photonic band gaps in one-dimensional dielectric plasma photonic crystals with a matching layer,” *Phys. Plasmas*, Vol. 19, 022103, 2012.
 27. Zhang, H. F., S. B. Liu, X. K. Kong, B. R. Bian, and Y. Dai, “Omnidirectional photonic band gap enlarged by one-dimensional ternary unmagnetized plasma photonic crystals based on a new Fibonacci quasiperiodic structure,” *Phys. Plasmas*, Vol. 19, 122102, 2012.
 28. Qi, L., Z. Yang, and T. Fu, “Defect modes in one-dimensional magnetized plasma photonic crystals with a dielectric defect layer,” *Phys. Plasmas*, Vol. 19, 012509, 2012.
 29. Zhang, H. F., S. B. Liu, and X. K. Kong, “Photonic band gaps in one-dimensional magnetized plasma photonic crystals with arbitrary declination,” *Phys. Plasmas*, Vol. 19, 122103, 2012.
 30. Hamidi, S. M., “Optical and magneto-optical properties of one-dimensional magnetized coupled resonator plasma photonic crystals,” *Phys. Plasmas*, Vol. 19, 012503, 2012.
 31. Mehdian, H., Z. Mohammadzahery, and A. Hasanbeigi, “Analysis

- of plasma-magnetic photonic crystals with a tunable band gap,” *Phys. Plasmas*, Vol. 20, 043505, 2013.
32. Qi, L., “Photonic band structures of two-dimensional magnetized plasma photonic crystals,” *J. Appl. Phys.*, Vol. 111, 073301, 2012.
 33. Zhang, H. F., X. K. Kong, and S. B. Liu, “Analysis of the properties of tunable prohibited band gaps for two-dimensional unmagnetized plasma photonic crystals under TM mode,” *Acta Physica Sinica*, Vol. 60, 055209, 2011.
 34. Zhang, H. F., S. B. Liu, and X. K. Kong, “Defect mode properties of two-dimensional unmagnetized plasma photonic crystals with line-defect under transverse magnetic mode,” *Acta Physica Sinica*, Vol. 60, 025215, 2011.
 35. Fu, T., Z. Yang, Z. Shi, F. Lan, D. Li, and X. Gao, “Dispersion properties of a 2D magnetized plasma metallic photonic crystals,” *Phys. Plasmas*, Vol. 20, 023109, 2013.
 36. Zhang, H. F., S. B. Liu, X. K. Kong, B. R. Bian, and Y. N. Guo, “Dispersion properties of two-dimensional plasma photonic crystals with periodically external magnetic field,” *Solid State Commun.*, Vol. 152, 1221–1229, 2012.
 37. Qi, L. and X. Zhang, “Band gap characteristics of plasma with periodically varying external magnetic field,” *Solid State Commun.*, Vol. 151, 1838–1841, 2011.
 38. Zhang, H. F., S. B. Liu, X. K. Kong, and B. R. Bian, “The characteristics of photonic band gaps for three-dimensional unmagnetized dielectric plasma photonic crystals with simple-cubic lattice,” *Optic Commun.*, Vol. 288, 82–90, 2013.
 39. Zhang, H. F., S. B. Liu, X. K. Kong, and B. R. Bian, “The properties of photonic band gaps for three-dimensional plasma photonic crystals in a diamond structure,” *Phys. Plasmas*, Vol. 20, 042110, 2013.
 40. Zhang, H. F., S. B. Liu, and X. K. Kong, “Dispersion properties of three-dimensional plasma photonic crystals in diamond lattice arrangement,” *J. Lightwave Technol.*, Vol. 17, 1694–1702, 2013.
 41. Zhang, H. F., S. B. Liu, and B. X. Li, “The properties of photonic band gaps for three-dimensional tunable photonic crystals with simple-cubic lattices doped by magnetized plasma,” *Optics & Laser Technology*, Vol. 50, 93–102, 2013.
 42. Zhang, H. F., S. B. Liu, H. Yang, and X. K. Kong, “Analysis of photonic band gap in dispersive properties of tunable three-dimensional photonic crystals doped by magnetized plasma,” *Phys. Plasmas*, Vol. 20, 032118, 2013.

43. Li, Z. Y., J. Wang, and B. Y. Gu, "Creation of partial gaps in anisotropic photonic-band-gap structures," *Phy. Rev. B*, Vol. 58, 3721–3729, 1998.
44. Malkova, N., S. Kim, T. Dilazaro, and V. Gopalan, "Symmetrical analysis of complex two-dimensional hexagonal photonic crystals," *Phys. Rev. B*, Vol. 67, 125203, 2003.
45. Li, Z. Y., B. Y. Gu, and G. Y. Yang, "Large absolute band gap in 2D anisotropic photonic crystals," *Phys. Rev. Lett.*, Vol. 81, 2574–2577, 1998.
46. Li, Z. and L. Lin, "Photonic band structures solved by a plane-wave-based transfer-matrix method," *Phys. Rev. E*, Vol. 67, 056702, 2003.
47. Marrone, M., V. F. Rodriguez-Esquerre, and H. E. Hernández-Figueroa, "Novel numerical method for the analysis of 2D photonic crystals: The cell method," *Opt. Exp.*, Vol. 10, 1299–1304, 2002.
48. Jun, S., Y. S. Cho, and S. Im, "Moving least-square method for the band-structure calculation of 2D photonic crystals," *Opt. Exp.*, Vol. 11, 541–551, 2003.
49. Chiang, P., C. Yu, and H. Chang, "Analysis of two-dimensional photonic crystals using a multidomain pseudospectral method," *Phys. Rev. E*, Vol. 75, 026703, 2003.
50. Lou, M., Q. H. Liu, and Z. Li, "Spectral element method for band structures of three-dimensional anisotropic photonic crystals," *Phys. Rev. E*, Vol. 80, 56702, 2012.
51. Zhang, H. F., S. B. Liu, X. K. Kong, L. Zhou, C. Z. Li, and B. R. Bo, "Comment on 'photonic bands in two-dimensional microplasma array. I. Theoretical derivation of band structures of electromagnetic wave'," *J. Appl. Phys.*, Vol. 110, 026104, 2011.